The WASCAL high-resolution regional climate simulation ensemble for West Africa: concept, dissemination, assessment

Dominikus Heinzeller[1], Diarra Dieng[1,2], Gerhard Smiatek[1], Christiana Olusegun[1], Cornelia Klein[3], Ilse Hamann[4], Seyni Salack[5], and Harald Kunstmann[1,2]

[1]Karlsruhe Institute of Technology, Institute of Meteorology and Climate Research, Garmisch-Partenkirchen, Germany
[2]University of Augsburg, Institute of Geography, Augsburg, Germany
[3]Natural Environment Research Council, Centre for Ecology & Hydrology, Wallingford, United Kingdom
[4]German Climate Computing Center, Hamburg, Germany
[5]WASCAL Competence Center, Ouagadougou, Burkina Faso

Correspondence to: Dominikus Heinzeller (heinzeller@kit.edu)

Abstract. Climate change and constant population growth pose severe challenges to 21st century rural Africa. Within the framework of the West African Science Service Center on Climate Change and Adapted Land Use (WASCAL), an ensemble of high-resolution regional climate change scenarios for the greater West African region are provided to support the development of effective adaptation and mitigation measures. This contribution presents the overall concept of the WASCAL regional climate simulations as well as detailed information on the experiment design, and provides information on the format and dissemination of the available data. All data is made available to the public at the CERA long-term archive of the German Climate Computing Center (DKRZ) with a subset available at the PANGAEA Data Publisher for Earth & Environmental Science portal (https://doi.pangaea.de/10.1594/PANGAEA.880512).

Regional climate projections are generated at high (12 km) and intermediate (60 km) resolution using the Weather Research & Forecasting Model (WRF). The simulations cover the validation period 1980–2010 and the two future periods 2020–2050 and 2070–2100. A brief comparison to observations and two climate change scenarios from the CORDEX initiative is presented to provide guidance on the data set to future users and to assess their climate change signal. Under the RCP4.5 scenario, the results suggest an increase in temperature by 1.5°C at the Coast of Guinea and by up to 3°C in the northern Sahel by the end of the 21st century, in line with existing climate projections for the region. They also project an increase in precipitation by up to 300 mm per year along the Coast of Guinea, by up to 150 mm per year in the Soudano region adjacent in the North, and almost no change in precipitation in the Sahel. This stands in contrast to existing regional climate projections, which predict increasingly drier conditions.

The high spatial and temporal resolution of the data, the extensive list of output variables, the large computational domain and the long time periods covered make this data set a unique resource for follow-up analyses and impact modelling studies over the greater West African region. The comprehensive documentation and standardisation of the data facilitate and encourage its use within and outside of the WASCAL community.

1 Introduction

With climate change being one of the most severe challenges to rural Africa in the 21st century, West Africa is facing an urgent need to develop effective adaptation and mitigation measures to protect its constantly growing population (Neumann et al., 2007; Naab et al., 2012; Eguavoen, 2013; Kirtman et al., 2013; Niang et al., 2014). WASCAL (West African Science Service Center on Climate Change and Adapted Land Use) is a large-scale research-focused program designed to help tackle this challenge and thereby enhance the resilience of human and environmental systems to climate change and increased variability. It does so by strengthening the research infrastructure and capacity in West Africa related to climate change and by pooling the expertise of ten West African countries and Germany [1]. Funded by the German Federal Ministry of Education and Research (BMBF), the research activities of WASCAL in Africa are coordinated by its Competence Center in Ouagadougou, Burkina Faso, supported by a Core Research Program in Germany under the leadership of the Center for Development Research (ZEF) at the University of Bonn. An integral part of the Core Research Program of WASCAL is the provisioning of a novel set of high-resolution regional climate projections for West Africa. In parallel, a climate observation network is set up in the region and significant efforts are made to compile a database of historical meteorological observations from various sources such as universities or meteorological and hydrological agencies across the WASCAL member countries.

Regional climate simulations have gained a significant amount of interest over the last years. The limited resolution of global circulation models (GCMs; typically around 1° or 110 km) prohibits the resolution of local, terrain-induced phenomena. Advances in computational power and in exploiting parallelism in numerical codes nowadays allow to run regional climate models (RCMs) at resolutions of 10km for predictions until 2100 (Bruyère, 2013). These RCMs can add significant value to global re-analyses and GCMs and in particular lead to an improved representation of the West African Monsoon (WAM). The dynamics of the WAM system are a consequence of complex interactions between dynamics, thermodynamics and surface conditions (Cook, 1999; Flaounas et al., 2012; Nicholson, 2013). In West Africa, where rainfall is limited to only few months per year, a correct representation of the WAM circulation and the associated onset and cessation of the rainy season are of utmost interest for farming management (Salack et al., 2016). In recent studies, Mounkaila et al. (2014) and Klein et al. (2015) showed that the ability of RCMs in simulating onset and cessation of the rainy season over West Africa strongly depends on how well the models reproduce the northward movement of the monsoon system and its associated features. Uncertainties also rise from the sparse observational network and the considerable differences in the derived gridded observation products for the region, against which models are validated and calibrated (Sylla et al., 2013).

---

[1]http://www.wascal.org

First high-resolution RCM studies over West Africa were conducted by Jung and Kunstmann (2007) using the mesoscale meteorological model MM5 (Grell et al., 1994) at 9 km resolution for two time slices 1991–2000 and 2030–2039 over a comparably small region covering the Volta Basin. They showed an annual mean temperature increase of around $1.3°C$ in the Volta region, significantly exceeding the inter-annual variability, and a mean annual change in precipitation from -20% to $+50\%$.

5   While an individual model run can provide a plausible representation of the future under a given climate change scenario, it does not allow an estimate of the range of outcomes expected for the assessment of risks and opportunities (Buontempo et al., 2015). Further, large uncertainties and errors are associated with the result of each model run as a consequence of imperfect initial conditions, the model being an imperfect abstraction of reality, and from numerical errors and artefacts accumulating in long-term simulations (for example, Laprise, 2003; Park et al., 2014).

10   Using an ensemble of climate simulations, these uncertainties can be reduced, and statistical estimates on projected future changes can be made at a considerable increase in computational costs. On global scale, the Coupled Model Intercomparison Project CMIP5 provides a framework for coordinated climate change experiments and contributed to the IPCC AR5 with a larger number of GCMs and future realisations (Taylor et al., 2012). For the region of West Africa, several regional ensemble modelling experiments were conducted in recent years (for example, Paeth et al., 2011). Current state of the art for the African

15   continent are long-term climate projections generated at a resolution of 50 km and for a large number of combinations of forcing data sets (i. e. GCMs) and RCMs within the Coordinated Regional Downscaling Experiment CORDEX (Giorgi et al., 2009). On shorter time scales, regional climate projections were generated for selected areas at a higher resolution of 25 km within CORDEX, employing 10 different RCMs (Nikulin et al., 2012). Spanning a significantly larger region, the RegCM4 model was used to downscale three different GCMs at the same horizontal resolution of 25 km (Sylla et al., 2015). A consistent

20   finding from these experiments was that the added value of the higher resolution provides an improved simulation of the annual cycle of precipitation and in regional differences in the response to global warming. An increased resolution allows for a more accurate representation of the coastline and topographic gradients and thus leads to a more realistic simulation along the Gulf of Guinea, amongst others.

    The work presented here advances the regional downscaling efforts for the region through the generation of a high-resolution,

25   ensemble regional climate simulation experiment for entire continental West Africa and large parts of the 21st century at a horizontal resolution of 12 km. Three GCMs are downscaled using the Weather Research and Forecasting tool (Skamarock et al., 2008) to narrow down uncertainties and provide estimates on the range of climate change impact on the region. A control run using re-analysis data as forcing is added to assess the RCM bias. The simulations provide a large set of output variables at very high temporal resolution to accommodate the needs for climate change analysis, impact modelling and further

30   downscaling experiments to convection-permitting resolutions. The model data generated in this experiment is made available for download to the public through two data portals to ensure easy access.

    In Sect. 2, we describe the design of our ensemble experiment and provide further details on the currently available data. Section 3 briefly illustrates the scientific value of these projections and assesses the validity of the chosen setup of this modelling experiment, while Sect. 4 provides details about the dissemination of the data. Section 5 is devoted to conclusions and an

35   outlook on the future modelling experiments.

2 Methods

2.1 Ensemble experiment design

The WASCAL ensemble presented here consists of a combination of three GCMs with one RCM for the green house gas scenario RCP4.5 (Representative Concentration Pathway 4.5; van Vuuren et al., 2011). The choice of RCP4.5 was made

5 because of limited computational resources and is based on the fact that (a) the differences between RCP4.5 and RCP8.5 become apparent only after 2040, and (b) that the RCP4.5 scenario – in light of the COP21 agreement made in Paris in December 2015 – is a reasonable scenario. The selected GCMs, on the other hand, cover the extremes in temperature and precipitation of the GCM ensemble used in CORDEX and span a larger range of conditions until about 2060 than the two scenarios and are able to reproduce the dominant, large-scale atmospheric features over West Africa (Nikulin et al., 2013;

10 Elguindi et al., 2014). Further, a control run using re-analysis data is included for model verification and future bias correction.

Table 7 summarises the forcing data sets and the limited area model employed in this ensemble experiment. The control run using re-analysis forcing data is conducted for the period 1979-2014. The historical runs are generated for the period 1979-2005 and extended by the RCP4.5 runs until 2010. This approach allows us to derive statistics for the climatological reference period 1980–2010, as defined by the World Meteorological Organization (2011). Future projections are calculated for the

15 periods 2019–2050 and 2069–2100 to provide similar 30-year windows for the mid and end of the 21st century. It should be noted that the three selected GCMs are based on different calendars, which makes model verification and comparison difficult on timescales shorter than one month: While the MPI-ESM MR model (as well as ERA-Interim) employs a Gregorian calendar, the GFDL-ESM2M and HadGEM2-ES models are based on a 365-day (no-leap year) and a 360-day (12×30 days) calendar, respectively.

20 The generation of an ensemble of climate projections at a resolution of 12 km and for at least 90 years in total is a process over several years and requires the use of different high performance computing (HPC) centres. To ensure consistency within each model run, the entire integration for a particular combination of GCM and RCM is conducted on the same system. Table 8 summarises the computational resources used in this ensemble experiment.

2.2 WRF model configuration

25 In limited area modelling, the size of the computational domain can have a significant influence on the quality of the results (Leduc and Laprise, 2008). In a recent study, Browne and Sylla (2012) demonstrated that the ability of a RCM to spin up the regional- and large-scale patterns associated with the West African Monsoon flow depend on a suitably large extent of the RCM domain. Figure 1 displays the nested domain configuration for the ensemble experiment, using an outer domain at 60 km resolution to downscale the coarse global forcing data sets and to provide boundary and initial conditions for the

30 inner domain at 12 km horizontal resolution. The figure also highlights the three dominant agro-climatological regions in West Africa, following a north-south gradient in annual precipitation. In addition to the domain configuration, a common standard for the model output was defined for all model runs to facilitate the use of the results. All data is provided in a netCDF CF-1.6

compliant format on a regular latitude-longitude grid for a pre-defined, extensive set of variables and pressure levels (see Sect. 4 for further details).

An inherent problem of limited area modelling is that supplying lateral boundary conditions to nested models can cause severe problems, up to the point where the RCM solution becomes inconsistent with the forcing data. This is problematic for long-term transient simulations associated with a large computational domain (Davies, 1983; Warner et al., 1997; Harris and Durran, 2010; Park et al., 2014). The different approaches to address this issue that are discussed in the literature range from daily to weekly re-initialisation, sometimes even including soil conditions (Otte, 2008), to transient runs covering the entire period of interest (Giorgi et al., 2009; Dieng et al., 2017). In general, more frequent re-initialisation is suitable for studying individual weather events, whereas a longer re-initialisation is useful in climate applications. Here, we adopt an intermediate solution by conducting 11-year time slice experiments, which allows for one year spin up of the soil conditions each time. For instance, the ERA-Interim-driven control run, providing data for the period 1980–2014, consists of the four time slice experiments 1979–1990, 1989–2000, 1999-2010, 2009–2014. Together with a spectral nudging approach on the outer domain (Miguez-Macho et al., 2004; von Storch et al., 2000; Otte et al., 2012), this approach allows the WRF model to spin up and evolve the necessary fine-scale structures, embedded in the large-scale features of the forcing global model, without departing too far from the global conditions.

An optimal configuration of the WRF model is paramount to address key questions regarding the impact of climate change. For the West African region, this equates to an accurate representation of the West African Monsoon (WAM) features in the model. In several studies it was shown that the choice of physical parameterisations available in WRF can greatly influence the model's skills, mostly measured in near-surface temperature and precipitation accuracy (Noble et al., 2014; Klein et al., 2015). For this experiment, we employ WRFV3.5.1 in a configuration summarised in Table 9. This setup is based on the Klein et al. (2015) WRF parameter study of 27 combinations of microphysics, planetary boundary layer and cumulus schemes for two extreme years (dry and wet), forced by ERA-Interim re-analysis data. To account for the different characteristics and resolutions of re-analysis data and GCM data, we extended their study and tested their most promising configurations using MPI-ESM MR (close to the CMIP5 multi model mean; Nikulin et al., 2013) as forcing data. The resulting optimal setup of WRF used in the WASCAL high-resolution ensemble experiment is thus a compromise to obtain good performance for both ERA-Interim and MPI-ESM MR forcing, and also accounts for the higher resolution (12 km versus 24 km in Klein et al., 2015).

WRFV3.5.1 supports Gregorian and 365-day calendar types, but not the 360-day calendar type employed by the HadGEM2-ES model. It was therefore necessary to add an implementation of the 360-day calendar to WRFV3.5.1. The 360-day calendar caused further complication to the pre-processing of the GCM data, since the grib standard does not support this calendar type.

The forcing model data was obtained from different sources and in different formats. ERA-Interim re-analysis data was downloaded from the European Centre for Medium-Range Forecasting ECMWF MARS archive[2], while MPI-ESM MR data was obtained from DKRZ's CERA archive[3], both in grib format. GFDL-ESM2M and HadGEM2-ES data was downloaded

---

[2]http://apps.ecmwf.int/mars-catalogue
[3]http://cera-www.dkrz.de

from the Earth System Grid Foundation (ESGF)[4] in netCDF format. This implied slightly different pre-processing steps for using the data as boundary conditions in WRF. For ERA-Interim and MPI-ESM MR, the standard pre-processing chain of WRF could be used, which consists of converting forcing model grib data to an intermediate format ("un-grib") used by the WRF preprocessing system WPS, which in turn is interpolated horizontally and vertically. For GFDL-ESM2M and HadGEM2-ES data, we implemented a separate tool to convert the netCDF data directly into the WPS intermediate format ("un-netcdf"), thereby avoiding the problem of an unsupported 360-day calendar in the grib standard.

To generate model output in a standard format, latest developments in the WRF model were employed and extended further: WRFV3.5.1 provides the capability to interpolate model-level data to pressure levels during the integration. This capability was extended to include additional variables (in particular hydrometeors). Further, climate diagnostics such as minimum and maximum daily temperatures are calculated using the climate diagnostics features of the model. While these interpolations require additional calculations during the integration that slow down the model integration, it was found that writing smaller amounts of data to disk (25 pressure levels instead of 40 model levels) overcompensated this increase and led to a faster model integration. The WRF model output was further post-processed by a suite of parallelised Python utilities to calculate additional variables, add CMIP5/CORDEX variable attributes and provide the desired netCDF-CF compliance.

3 Assessment

In this section, we present a qualitative overview of the different WRF model runs and provide guidance to future users of the data. It is also meant to assess the assumptions on the basis of which the ensemble experiment was designed, e. g. the characteristics of the different forcing models mentioned in the previous section.

Figure 2 displays the annual cycle of mean near-surface temperatures for the historical reference period 1980–2010, the near future 2020–2050 and the end of the century 2070–2100. For the historical period, observations are obtained from the University of Delaware at 0.5° resolution (55 km, UDEL v3.01; Willmott and Matsuura, 2012). Also displayed are data from the AgMERRA Climate Forcing Datasets for Agricultural Modeling at 0.25° resolution (27 km, AgMERRA; Rienecker et al., 2011). The WASCAL climate change projections are displayed at 60 km and 12 km resolution for the different model runs WRF-R (forced by ERA-Interim), WRF-M (MPI-ESM MR), WRF-G (GFDL-ESM2M), WRF-H (HadGEM2-ES) and the WRF multi-model ensemble WRF-E, composed of the three GCM-driven runs WRF-M, WRF-G and WRF-H.

The AgMERRA dataset matches closely with the observations in all regions and throughout the year. Averaged over the different areas and on a monthly timescale, the differences between the 60 km and 12 km runs for the same forcing data set are small, compared to differences between model runs with the same resolution and different forcing data sets. The re-analysis run WRF-R agrees with the observations for most parts of the year, except for the height of the monsoon season (July–September), for which the observations show a dip in temperatures that is absent in the WRF-R run. For the Soudano area (see Fig. 1), the WRF-R run shows a larger positive bias than for the other regions. The multi-model ensemble WRF-E shows a cold bias of ∼2–4°C for most parts of the year except during the monsoon season, where it matches the observed temperatures closely. The

---

[4]http://www.earthsystemgrid.org

individual components of the ensemble are characterised by WRF-G being consistently colder, WRF-H being close to, and WRF-M being consistently warmer than WRF-E. Among the three GCM-driven runs, WRF-M fits the observed temperatures best. With respect to future conditions, all model runs show increasing temperatures by 2.5–3°C on average until the end of the century, with WRF-H exhibiting the strongest climate change signal (∼4°C) and WRF-G the weakest (<2°C).

5   In a similar fashion, Fig. 3 displays the annual cycle of monthly precipitation. Again, AgMERRA fits the observations from UDEL closely. The difference between the 12 km and 60 km WRF runs is larger for precipitation than it is for temperature, with a tendency to generate more precipitation in the higher-resolution runs than the lower-resolution runs. This is true for all cases except between July and October along the Coast of Guinea. In this particular case, the high-resolution runs, and foremost the WRF-R run, show a distinct drop in precipitation that is absent in the lower-resolution runs and in the observations/re-
10   analysis. All WRF runs tend to overestimate precipitation between February and June along the Coast of Guinea and for entire continental West Africa (labelled as "land") in general, with WRF-R showing the largest excess in precipitation and and WRF-G matching the observations best. Among the three GCM-driven ensemble members, WRF-M tends to highest and WRF-G to lowest precipitation amounts, while WRF-H lies in between. Consequently, WRF-E overpredicts precipitation slightly along the coast of Guinea and matches the observations well in the Soudano and Sahel regions. With respect to future conditions,
15   all WRF ensemble members show an increase in precipitation along the Coast of Guinea and to some extent in the Soudano region, whereas almost no change can be detected for the Sahel. As for temperature, WRF-H shows the largest and WRF-G the smallest climate change signal.

Figures 4 and 5 display spatial distributions of annual mean near-surface temperature and annual precipitation at 12 km and 60 km resolution for the re-analysis runs WRF-R, the multi-model ensemble WRF-E, an additional high-resolution (12 km)
20   re-analysis run with the CCLM regional climate model, obtained within the WASCAL programme (Dieng et al., 2017), and a two-member ensemble from CORDEX (Giorgi et al., 2009) at 50 km resolution. The two CORDEX simulations use the regional model RCA4 (Strandberg et al., 2014) to downscale MPI-ESM LR and GFDL-ESM2M forcing data. These simulations were chosen because of their similar/identical forcing models. Also shown are differences of these data sets with respect to AgMERRA at 27 km resolution. To calculate these differences, all data sets were remapped to the 12 km grid of the high-resolution
25   WRF simulations.

With respect to temperature, beyond the findings discussed above, the spatial plots reveal a distinct bipolar cold bias at approximately the location of the Saharan Heat Low (SHL; 20°N, 5°W) and 15° east of it. This feature is present in all WRF, CCLM and CORDEX runs. The spatial patterns of all WRF runs are similar and show relatively higher temperatures in the Soudano region, leading to a warm bias in WRF-R and nearly no bias in WRF-E over this region. The warm belt present in the
30   WRF runs around 10°N is confined to west of the Meridian in the CCLM-R run and absent in the CORDEX runs.

For precipitation, the spatial plots shed further light on the zonal distribution of precipitation and the biases relative to AgMERRA. All WRF runs tend to a dry bias along the south-west coast of Guinea, Sierra Leone and Liberia, presumably related to the complex interplay of onshore winds, the coastline and the elevated topography of the Guinea Highlands. Further to the east, the WRF runs tend towards a wet bias, in particular the re-analysis run WRF-R. The CCLM-R run, on the contrary,
35   displays a strong dry bias along the entire coastline and further inland, while the CORDEX runs exhibit a wet bias in most

parts of the domain. North of 15° latitude, the WRF and CCLM runs fit observed precipitation well, while the CORDEX runs still show a wet bias.

Figures 6 and 7 display spatial distributions of the climate change signal on temperature and precipitation for the WRF multi-model ensemble WRF-E and the RCA4 ensemble from CORDEX. With respect to temperature, the WRF ensemble shows a
5 gradient in warming, running from South to North and ranging between 1.5°C at the Coast of Guinea to 3°C in Mauritania and northern Mali. The CORDEX runs display a gradient running from Southwest to Northeast between 1.5°C and 2.5°C. For precipitation, the differences between the WASCAL WRF runs and the CORDEX RCA4 runs is more pronounced. This can be partly attributed to the fact that the CORDEX RCA4 ensemble used here lacks a HadGEM2-driven member, which, amongst the three WRF runs, shows the strongest climate change signal. The WRF ensemble shows a clearly wetter future for
10 the Coast of Guinea (up to 300 mm per year) and the Soudano region (up to 200 mm per year), and slightly higher amounts of precipitation in the Sahel region than at present. The CORDEX runs predict larger amounts of annual precipitation only along the southwestern Coast of Guinea, a slight drying over Nigeria and no precipitation changes otherwise.

4 Data availability

The data is provided in a netCDF CF-1.6 compliant format using netCDF4 compression. All data is interpolated to a regular
15 latitude-longitude grid for a pre-defined, extensive set of variables and pressure levels. The data is organised in streams with different output intervals as a compromise between the requirements of follow-up studies and storage constraints. A surface stream bundles all variables at and below the surface at 3-hourly intervals, whereas pressure-level variables are provided every 6 hours on 25 levels in a pressure stream. Climate diagnostics such as minimum/maximum temperatures are provided daily in a climate stream, and time-invariant information such as landcover and terrain height are collected in a static stream. The naming
20 convention adopted here follows closely the CMIP5 and CORDEX conventions. All data is made available to the public via two different portals. The full data set, i. e. all variables at full temporal and spatial resolution, can be obtained from the CERA database at DKRZ (Heinzeller et al., 2017a, see also Table 10)[5]. A subset of the data at daily and monthly temporal resolution is also made available through the PANGAEA Data Publisher for Earth & Environmental Science portal (Heinzeller et al., 2017b, see also Table 10)[6]. The WASCAL climate simulation data is freely accessible to all users, albeit CERA requires a user
25 registration. A full description of the available data and the file naming conventions is provided in the appendix, and alongside with the data on CERA[7] and on PANGAEA[8].

---

[5]https://cera-www.dkrz.de/WDCC/ui/cerasearch

[6]https://www.pangaea.de

[7]https://cera-www.dkrz.de/WDCC/ui/Entry.jsp?acronym=WASCAL_WRF_README

[8]https://doi.pangaea.de/10013/epic.51574.d001

5   Conclusions and outlook

A novel set of high- and medium-resolution climate change simulations for the greater West African region is provided to the research community within the framework of WASCAL, which advances significantly beyond currently available data sets. The ensemble uses the Weather Research & Forecasting Model WRF to downscale three different global circulation models for three 30-year periods between 1980 and 2100, completed by a re-analysis driven control run for the historical period 1980–2014. These data sets are made available freely through different data portals. A standardised and documented data structure, closely following the CMIP5 and CORDEX conventions, is adopted to foster easy and quick use of the data and effective collaboration. Apart from the higher spatial resolution (12 km and 60 km) than existing regional climate change experiments (25–50 km; Giorgi et al., 2009; Sylla et al., 2016) or global simulations (100-200 km; Taylor et al., 2012), our data is provided at high temporal resolution (3-hourly, 6-hourly, daily) on 25 pressure levels and four subsurface levels. A large number of 76 output variables in total are available to enable a diversity of climate change analyses, impact modelling studies and further downscaling to convection-permitting resolutions.

It is important to note that the brief analysis presented here is performed on monthly and annual timescales, averaged over 30-year time slices, and compared to observations and re-analysis data at ∼30 km resolution. A detailed analysis of the data using observational data sets at high temporal and spatial resolution (where available), focussing on local-scale features, is beyond the scope of this contribution. The main characteristics of the WRF simulations can be summarised as follows: In general, our WRF setup tends to increase both temperature and precipitation amounts, compared to the original forcing data set. These positive biases, in combination with the characteristics (i. e. biases) of the forcing data sets (Table 7) lead to an overall positive bias of the ERA-Interim driven WRF runs in temperature and precipitation. For the MPI-ESM MR driven WRF runs, they imply a good agreement with respect to temperature, alongside with a positive bias in precipitation. Conversely, for the GFDL-ESM2M driven WRF runs, they lead to a good agreement with respect to precipitation and a large negative bias in temperature. The HadGEM2-ES driven WRF runs lie in between for both temperature and precipitation.

With respect to climate change, the WRF simulations project an increase in temperature between 1.5°C and 3°C, with higher values in the Sahel, in an overall agreement with existing global and regional climate projections (Giorgi et al., 2009; Taylor et al., 2012; Sylla et al., 2016). For precipitation, our simulations project an increase in precipitation between 150 mm and 300 mm per year all south of 15°N, in line with the majority of the CMIP5 models (for example, Lee and Wang, 2014). However, this stands in contrast to existing regional climate modelling studies, for example the findings of Sylla et al. (2016), who analysed the response of West African climate zones to anthropogenic climate change in the late 21st century. Based on ensemble data from CORDEX and their own higher-resolution RegCM4 experiments, they concluded that West Africa evolves towards increasingly torrid, arid and semi-arid conditions. These contradicting signals do highlight the large uncertainty in projected future rainfall, even on continental scale.

The WRF simulations in this WASCAL high-resolution ensemble are conducted as time-slice experiment over ten years, preceded by an additional year for model spin up. As discussed in Bruyère et al. (2016) and Lucas-Picher et al. (2008), the internal variability of regional models is generally small compared to the interannual variability in decadal simulations. On the

other hand, it is less clear whether differences between individual 10-year periods are dominated by climate variability rather than climate change. We therefore advocate to utilise the entire 30-year periods, each consisting of three consecutive decadal simulations, for the present day (1980–2010), the near-future (2030–2050) and the distant future (2070–2100). To do so, the spin up period of one year for each of the decadal runs has to be neglected.

5   Despite its widespread use, classical limited area modelling as it is used in the regional downscaling experiments presented here suffers from several limitations such as numerical artefacts at domain and nest boundaries, diverging solutions between the regional model and the global forcing model, and the inability to provide feedback from the regional to the forcing model, to name a few. Alternative modelling systems such as the global Model for Prediction Across Scales (MPAS; Skamarock et al., 2012) make use of innovative variable-resolution mesh geometries with smooth transitions between different areas of

10 refinement and provide excellent scaling on modern high performance computing systems. MPAS was tested recently, using uniform and variable resolution meshes over the region of West Africa, and showed promising results (Heinzeller et al., 2016). For instance, the 60-12 km variable-resolution mesh used in their study (i.e. with a 60 km resolution globally and a 12 km resolution over the entire North African continent) shows a clear bipolar pattern of high temperatures in the locations where all of the regional climate simulations presented here exhibit a cold bias (Fig. 4 here versus Figs. 9 and 11 in Heinzeller et al.,

15 2016). This could be related to an improved representation of large scale patterns governing the West African climate in global models and requires further investigation.

Within the framework of WASCAL, additional high-resolution climate simulations are carried out, employing other regional climate models such as CCLM (Dieng et al., 2017) or focusing on specific areas such as the agriculturally important Volta Basin (Annor et al., 2017). Also, to improve the representation of the diurnal cycle of precipitation and of extreme precipitation events

20 in the models, convection-permitting and coupled atmospheric-hydrological modelling experiments are pursued (Arnault et al., 2016; Klein et al., 2017; Naabil et al., 2017). The climate modelling efforts presented here are undertaken in parallel to the set-up of a dense network of automatic weather stations in the region with the goal to assess and reduce model uncertainties and biases. Together, the modelling and observational activities of WASCAL will enable researchers and stakeholders to develop effective climate change mitigation measures for West Africa with a higher level of confidence from local to continental scale.

Appendix A: Additional information on the WASCAL WRF climate simulation data

25

The full description of the available data and the file naming conventions provided in this appendix are identical to the information contained in the WASCAL_WRF_README on CERA (https://cera-www.dkrz.de/WDCC/ui/Entry.jsp?acronym=WASCAL_WRF_README) and on PANGAEA (https://doi.pangaea.de/10013/epic.51574.d001).

A1   Description of variables

30 Table A1 summarises the list of output variables of the WASCAL climate simulations. The table includes all variables that are produced by the WRF model runs. Static variables are provided only once in the static output stream. For further information

on the meaning and calculation of these fields, the user is referred to the WRF Users' Guide, in particular to chapter 5[9]. The variable types are "acc" (accumulated values), "coord" (coordinate variables), "const" (constant values), "min" (minimum over last output interval), "max" (maximum over last output interval) and "inst" (instantaneous values). The variables are classified into different streams with different output frequency (see Sect. A2 below).

5   **Note 1.** The climate output diagnostic variables contained in stream wrfclm are only available for the high-resolution (12 km) experiments, not for the low-resolution (60 km) experiments.

Note 2. The following time-slice experiments are missing the accumulated radiation budgets (rlds, rldt, rlus, rlut, rsds, rsdt, rsus, rsut; see Sect. A4 and A5 for details on the time slices and naming conventions): WRF12_MPIESM_HIST/{1979-1990, 1999-2006}, WRF12_MPIESM_RCP45/{2006-2010, 2039-2050, 2089-2100}.

10   ## A2   Description of streams

The output variables are classified into different output streams, which are described in Table A2. The streams have different output frequencies. Note that the stream classification does not appear in the directory structure or file names (see Sect. A4 below).

A3   Pressure levels for stream wrfprs

15   The native model output is interpolated to 25 pressure levels, see Table A3. Variables on pressure levels are set to missing values below ground.

A4   Description of files

The data is provided in compressed netCDF4 format, CF-1.6 compliant. All data is combined into monthly output files, independent of the output frequency and size of the variables. The coarser 60 km runs provide the same data as the 12 km, runs
20   except for the climate output diagnostics (stream wrfclm is not present). A consistent filename convention is adopted and described in Table A4.

A5   Description of nesting strategy and time-slices

The domain configuration is displayed and described in detail in the main text. The high-resolution runs (12 km) are carried out as a nested simulation, using the output of the coarser resolution (60 km) model runs as forcing data set. The coarser model
25   runs are forced by the different re-analysis and GCM data sets described above. An offline-nesting approach is adopted, which implies no feedback from the 12 km experiments to the 60 km experiments. Thus, the 60 km experiments can be considered as standalone experiments at a relatively coarse resolution.

The experiments are conducted as time-sliced runs of 11 year duration each, where the first year is considered as spinup period and should not be used in the analysis. The historical run 1999-2006 is carried over into the projection run 2006–

---

[9]http://www2.mmm.ucar.edu/wrf/users/docs/user_guide_V3/users_guide_chap5.htm

2010 to be able to provide model data for the WMO reference period 1980–2010 by combining the three decadal time-slice experiments 1979–1990, 1989–2000, 1999–2010 and neglecting the spinup year for each of them. The available time slices are summarised in Table A5.

A6 Subset of data available at PANGAEA

5 To facilitate the use of the WASCAL data for applications that do not require the full set of variables or the full temporal resolution of the data, a subset of the dataset available at CERA is provided through the PANGAEA portal. This subset is derived from the data provided at CERA as follows:

1. Only data from the high-resolution 12 km runs are considered, not from the intermediate-resolution 60 km runs.

2. A subset of variables of potentially high interest are selected (see Table A6).

10 3. Accumulated data (rainfall, radiation budgets are de-accumulated into precipitation sums and radiation averages between two output time steps).

4. Data at high temporal resolution (3-hourly, 6-hourly) are aggregated to daily or monthly timescales.

5. Atmospheric variables on pressure levels are extracted for 11 out of the 25 available pressure levels (see Table A6).

6. Data are concatenated into 30-year periods 1980–2010 (control, historical), 2020–2050 (RCP4.5), 2070–2100 (RCP4.5), 15 thereby neglecting the 1-year spinup period for each of the time-slice experiments.

7. A slightly different file naming convention is adopted to reflect the above modifications of the data (see Table A6).

Note 1. The accumulated radiation budgets are missing for the runs using MPIESM as forcing data set (see also Sect. A1).

Note 2. For the periods 1980–2010, the historical runs 1999–2005 are completed by the (continuation) runs 2006–2010 from the RCP4.5 scenario, but the 30-year data sets are labelled as "historical".

20 ## A7 Rights of use

The data is provided under the Creative Commons license 4.0. For details about the licensing model, see the following web page: https://creativecommons.org/licenses/by/4.0/.

A8 Liability/Warranty

1. The data are made available to the user without any warranty. The user is aware that the data have been obtained according 25 to current state-of-the-art science and computational engineering.

2. The data producer must not be taken into any obligation to third parties on the basis of this agreement. Any liability of the data producer for damage of all kinds resulting from the provision and further processing of the data is ruled out. The user indemnifies the data producer from any liability to damaged third parties.

3. The liability disclaimer stated under (1) and (2) does not apply insofar as the data producer has acted in gross negligence or with wilful intent.

Table A1: List of output variables of the WASCAL WRF climate simulations. The variable types are "acc" (accumulated values), "coord" (coordinate variables), "const" (constant values), "min" (minimum over last output interval), "max" (maximum over last output interval) and "inst" (instantaneous values).

WRF name	Output name	Units	Stream	Type	Description (long name)
ACLWDNB	rlds	J m-2	wrfsfc	acc	Accumulated surface downwelling longwave radiation
ACLWDNT	rldt	J m-2	wrfsfc	acc	Accumulated TOA incident longwave radiation
ACLWUPB	rlus	J m-2	wrfsfc	acc	Accumulated surface upwelling longwave radiation
ACLWUPT	rlut	J m-2	wrfsfc	acc	Accumulated TOA outgoing longwave radiation
ACSWDNB	rsds	J m-2	wrfsfc	acc	Accumulated surface downwelling shortwave radiation
ACSWDNT	rsdt	J m-2	wrfsfc	acc	Accumulated TOA incident shortwave radiation
ACSWUPB	rsus	J m-2	wrfsfc	acc	Accumulated surface upwelling shortwave radiation
ACSWUPT	rsut	J m-2	wrfsfc	acc	Accumulated TOA outgoing shortwave radiation
ALBEDO	alb	1	wrfsfc	inst	Albedo
CANWAT	canwat	kg m-2	wrfsfc	inst	Canopy water
CLDFRA	cl	1	wrfprs	inst	Cloud area fraction
DEPTH	depth	m	wrfsfc	coord	Depth
EMISS	ems	1	wrfsfc	inst	Surface emissivity
GHT	zg	m	wrfprs	inst	Geopotential height
GRDFLX	hfg	W m-2	wrfsfc	inst	Ground heat flux
HFX	hfss	W m-2	wrfsfc	inst	Surface upward sensible heat flux
HGT	orog	m	wrfsta	inst	Terrain height
ISLTYP	sltype	1	wrfsta	const	Dominant soil category
IVGTYP	vegtype	1	wrfsta	const	Dominant vegetation category
LANDMASK	sftlf	1	wrfsta	const	Land binary mask (1 for land, 0 for water)
LAT	lat	degrees_north	wrfclm, wrfprs, wrfsfc, wrfsta	coord	Latitude, south is negative
LH	hfls	W m-2	wrfsfc	inst	Surface upward latent heat flux
LON	lon	degrees_east	wrfclm, wrfprs, wrfsfc, wrfsta	coord	Longitude, west is negative
MU	amdry	Pa	wrfsfc	inst	Dry air mass in column
PBLH	zmla	m	wrfsfc	inst	Atmosphere boundary layer thickness
PLEV	plev	hPa	wrfprs	coord	Pressure

Continued on next page

Continued from previous page

WRF name	Output name	Units	Stream	Type	Description (long name)
PMSL	psl	Pa	wrfsfc	inst	Sea level pressure
PSFC	ps	Pa	wrfsfc	inst	Surface air pressure
Q2	vaps	kg kg-1	wrfsfc	inst	Near-surface water vapor mixing ratio
QCLOUD	clw	kg kg-1	wrfprs	inst	Cloud water mixing ratio
QFX	mfs	kg m-2 s-1	wrfsfc	inst	Surface upward moisture flux
QICE	cli	kg kg-1	wrfprs	inst	Ice mixing ratio
QRAIN	clr	kg kg-1	wrfprs	inst	Rain water mixing ratio
QSNOW	cls	kg kg-1	wrfprs	inst	Snow mixing ratio
QVAPOR	vap	kg kg-1	wrfprs	inst	Water vapor mixing ratio
RAIN	pr	mm	wrfsfc	acc	Accumulated precipitation
RH	hur	%	wrfprs	inst	Relative humidity
RH2	hurs	%	wrfsfc	inst	Near-surface relative humidity
SEAICE	sic	1	wrfsfc	inst	Sea ice binary mask (1 for sea ice, 0 for water)
SHDMAX	vegmax	1	wrfsta	const	Annual max vegetation fraction
SHDMIN	vegmin	1	wrfsta	const	Annual min vegetation fraction
SKINTEMPMAX	tsmax	K	wrfclm	max	Daily maximum surface skin temperature
SKINTEMPMIN	tsmin	K	wrfclm	min	Daily minimum surface skin temperature
SMCREL	mrrlsl	1	wrfsfc	inst	Relative soil moisture
SMOIS	mrlsl	m3 m-3	wrfsfc	inst	Water content of soil layer
SMOIST	mrso	m3 m-3	wrfsfc	inst	Total soil moisture content
SNOALB	albmax	1	wrfsta	const	Annual max snow albedo in fraction
SNOW	snw	kg m-2	wrfsfc	inst	Snow water equivalent
SNOWH	snd	m	wrfsfc	inst	Physical snow depth
SPDUV	wind	m s-1	wrfprs	inst	Wind speed
SPDUV10	sfcWind	m s-1	wrfsfc	inst	Near-surface wind speed
SPDUV10MAX	sfcWindmax	m s-1	wrfclm	max	Daily maxmimum near-surface wind speed
SR	prfz	1	wrfsfc	inst	Fraction of frozen precipitation
SST	tso	K	wrfsfc	inst	Sea surface temperature
SWDDIF	swddif	W m-2	wrfsfc	inst	Shortwave surface downward diffuse irradiance
SWDDIR	swddir	W m-2	wrfsfc	inst	Shortwave surface downward direct irradiance
SWDDNI	swddni	W m-2	wrfsfc	inst	Shortwave surface downward direct normal irradiance
T	ta	K	wrfprs	inst	Air temperature
T2	tas	K	wrfsfc	inst	Near-surface air temperature
T2MAX	tasmax	K	wrfclm	max	Daily maximum near-surface air temperature
T2MIN	tasmin	K	wrfclm	min	Daily minimum near-surface air temperature

Continued from previous page

WRF name	Output name	Units	Stream	Type	Description (long name)
TCLDFRA	clt	1	wrfsfc	inst	Total cloud fraction
TD	td	K	wrfprs	inst	Dew point temperature
TD2	tds	K	wrfsfc	inst	Near-surface dew point temperature
TH2	thetas	K	wrfsfc	inst	Near-surface potential temperature
TIME	time	hours since 1970-01-01	wrfclm, wrfprs, wrfsfc, wrfsta	inst	Time
TMN	tsll	K	wrfsfc	inst	Temperature of soil at lower boundary
TSK	ts	K	wrfsfc	inst	Surface skin temperature
TSLB	tsl	K	wrfsfc	inst	Temperature of soil
U	ua	m s-1	wrfprs	inst	Eastward wind
U10	uas	m s-1	wrfsfc	inst	Eastward near-surface wind
U10MAX	uasmax	m s-1	wrfclm	max	Daily maximum eastward near-surface wind
V	va	m s-1	wrfprs	inst	Northward wind
V10	vas	m s-1	wrfsfc	inst	Northward near-surface wind
V10MAX	vasmax	m s-1	wrfclm	max	Daily maximum northward near-surface wind
VEGFRA	veg	1	wrfsfc	inst	Vegetation fraction
W	wa	m s-1	wrfprs	inst	Upward wind

Table A2. Description of streams into which the WASCAL WRF output variables are classified.

Stream name	Description	Output interval
wrfclm	climate variables (extremes), two-dim.	day
wrfprs	pressure level variables, three-dim.	6hr
wrfsfc	surface, subsurface and other two-dim. variables	3hr
wrfsta	static variables, two-dim.	fx

Table A3. Pressure levels to which 3-dimensional atmospheric variables are interpolated.

Pressure levels [hPa]
1000, 975, 950, 925, 900, 850, 800, 750, 700, 650, 600, 550, 500, 450, 400, 350, 300, 250, 200, 150, 100, 70, 50, 30

Table A4. File naming convention for the WASCAL WRF ensemble. Here, {sr} denotes the spatial resolution in km, {forcing} the forcing model, {scenario} the scenario, {var} the variable, {yyyy}–{mm} the year and month, and {tr} the output interval (temporal resolution).

Filename pattern:	wrf{sr}_{forcing}_{scenario}_{var}_{yyyy}-{mm}_{tr}.nc
Example 1:	wrf12_eraint_ctrl_tasmax_1982-12_fx.nc
Example 2:	wrf12_mpiesm_rcp45_sftlf_2029-01_day.nc
Example 3:	wrf60_gfdlesm_hist_ta_2003-04_6hr.nc
Example 4:	wrf60_hadgem2_rcp45_tas_2099-12_3hr.nc

Table A5. Description of time-slices generated in the WASCAL WRF ensemble experiment, including spinup period.

Scenario	Time-slices
Control (ctrl)	1979–1990, 1989–2000, 1999–2010, 2009–2014
Historical (hist)	1979–1990, 1989–2000, 1999–2005 (continued by 2006–2010)
Projection (rcp4.5)	2006–2010 (continued from 1999–2005), 2019–2030, 2029–2040, 2039–2050, 2069–2080, 2079–2090, 2089–2100

Table A6. Subset of data available at PANGAEA. The variables and de-accumulation steps are described in Sects. A1 and A6, the parameters enclosed in curly brackets in Sect. A4.

Variables	
de-accumulated, daily sums/averages	pr, rlds, rldt, rlus, rlut, rsds, rsdt, rsus, rsut
daily averages	hfls, hfss, hurs, mrso, psl, tas, tasmax, tasmin, tds
monthly averages	swddif, swddir, swddni, ua, va, wa, zg
Pressure levels [hPa]	
for variables ua, va, wa, zg	1000, 850, 750, 700, 650, 600, 550, 450, 350, 250, 150
Naming convention	
de-accumulated variables, daily sums	DAC_wa12clmN_{forcing}_{scenario}_{var}_{yyyy}_{yyyy}_DAYSUM.nc
de-accumulated variables, daily averages	DAC_wa12clmN_{forcing}_{scenario}_{var}_{yyyy}_{yyyy}_DAYMEAN.nc
other variables, daily averages	wa12clmN_{forcing}_{scenario}_{var}_{yyyy}_{yyyy}_DAYMEAN.nc
other variables, monthly averages	wa12clmN_{forcing}_{scenario}_{var}_{yyyy}_{yyyy}_MONMEAN.nc

Competing interests. No competing interests are present.

Earth System
Open Access
Science
Data
Discussions

References

Annor, T., Lamptey, B., Wagner, S., Oguntunde, P., Arnault, J., Heinzeller, D., and Kunstmann, H.: High-resolution long-term WRF climate simulations over Volta Basin. Part 1: validation analysis for temperature and precipitation, Theoretical and Applied Climatology, pp. 1–21, https://doi.org/10.1007/s00704-017-2223-5, http://link.springer.com/10.1007/s00704-017-2223-5, 2017.

5 Anon, A.: GFDL's ESM2 Global Coupled Climate-Carbon Earth System Models. Part I: Physical Formulation and Baseline Simulation Characteristics, Journal of Climate, 25, 6646–6665, https://doi.org/http://dx.doi.org/10.1175/JCLI-D-11-00560.1, 2012.

Arnault, J., Wagner, S., Rummler, T., Fersch, B., Bliefernicht, J., Andresen, S., and Kunstmann, H.: Role of runoff-infiltration partitioning and resolved overland flow on land-atmosphere feedbacks: A case-study with the WRF-Hydro coupled modeling system for West Africa, Journal of Hydrometeorology, p. 151123135311007, https://doi.org/10.1175/JHM-D-15-0089.1, http://journals.ametsoc.org/doi/abs/10.

10 1175/JHM-D-15-0089.1, 2016.

Browne, N. A. K. and Sylla, M. B.: Regional climate model sensitivity to domain size for the simulation of the West African summer monsoon rainfall, International Journal of Geophysics, 2012, https://doi.org/10.1155/2012/625831, 2012.

Bruyère, C.: Regional Climate Research using WRF and MPAS: Overview and Future Development, 2013.

Bruyère, C., Raktham, C., Done, J., Kreasuwun, J., Thongbai, J., and Promnopas, W.: Major weather regime changes over Southeast Asia in

15 a near-term future scenario, Climate Research, https://doi.org/10.3354/cr01442, http://www.int-res.com/prepress/c01442.html, 2016.

Buontempo, C., Mathison, C., Jones, R., Williams, K., Wang, C., and McSweeney, C.: An ensemble climate projection for Africa, Climate Dynamics, 44, 2097–2118, https://doi.org/10.1007/s00382-014-2286-2, 2015.

Cook, K. H.: Generation of the African easterly jet and its role in determining West African precipitation, Journal of Climate, 12, 1165–1184, https://doi.org/10.1175/1520-0442(1999)012<1165:GOTAEJ>2.0.CO;2, 1999.

20 Davies, H. C.: Limitations of Some Common Lateral Boundary Schemes used in Regional NWP Models, Monthly Weather Review, 111, 1002–1012, https://doi.org/10.1175/1520-0493(1983)111<1002:LOSCLB>2.0.CO;2, 1983.

Dee, D. P., Uppala, S. M., Simmons, A. J., Berrisford, P., Poli, P., Kobayashi, S., Andrae, U., Balmaseda, M. A., Balsamo, G., Bauer, P., Bechtold, P., Beljaars, A. C. M., van de Berg, L., Bidlot, J., Bormann, N., Delsol, C., Dragani, R., Fuentes, M., Geer, A. J., Haimberger, L., Healy, S. B., Hersbach, H., Hólm, E. V., Isaksen, L., Kållberg, P., Köhler, M., Matricardi, M., Mcnally, A. P., Monge-Sanz,

25 B. M., Morcrette, J. J., Park, B. K., Peubey, C., de Rosnay, P., Tavolato, C., Thépaut, J. N., and Vitart, F.: The ERA-Interim reanalysis: Configuration and performance of the data assimilation system, Quarterly Journal of the Royal Meteorological Society, 137, 553–597, https://doi.org/10.1002/qj.828, 2011.

Dieng, D., Smiatek, G., Bliefernicht, J., Heinzeller, D., Sarr, A., Gaye, A. T., and Kunstmann, H.: Evaluation of the COSMO-CLM high-resolution climate simulations over West Africa, Journal of Geophysical Research: Atmospheres, 122, 1437–1455,

30 https://doi.org/10.1002/2016JD025457, 2017.

Eguavoen, I.: Climate change and trajectories of blame in northern ghana, Anthropological Notebooks, 19, 5–24, 2013.

Elguindi, N., Giorgi, F., and Turuncoglu, U.: Assessment of CMIP5 global model simulations over the subset of CORDEX domains used in the Phase I CREMA, Climatic Change, 125, 7–21, https://doi.org/10.1007/s10584-013-0935-9, 2014.

Flaounas, E., Janicot, S., Bastin, S., Roca, R., and Mohino, E.: The role of the Indian monsoon onset in the West African monsoon onset:

35 Observations and AGCM nudged simulations, Climate Dynamics, 38, 965–983, https://doi.org/10.1007/s00382-011-1045-x, 2012.

Giorgi, F., Jones, C., and Asrar, G. R.: Addressing climate information needs at the regional level: the CORDEX framework, Bulletin - World Meteorological Organization, 58, 175–183, 2009.

Grell, G. A., Dudhia, J., and Stauffer, D. R.: A description of the Fifth-generation Penn State/NCAR Mesoscale Model (MM5), NCAR Technical Note NCAR/TN-398+STR, p. 121, https://doi.org/10.5065/D60Z716B, 1994.

Harris, L. M. and Durran, D. R.: An Idealized Comparison of One-Way and Two-Way Grid Nesting, Monthly Weather Review, 138, 2174–2187, https://doi.org/10.1175/2010MWR3080.1, 2010.

5 Heinzeller, D., Duda, M. G., and Kunstmann, H.: Towards convection-resolving, global atmospheric simulations with the Model for Prediction Across Scales (MPAS) v3.1: An extreme scaling experiment, Geoscientific Model Development, 9, 77–110, https://doi.org/10.5194/gmd-9-77-2016, 2016.

Heinzeller, D., Dieng, D., Smiatek, G., Olusegun, C., Klein, C., Hamann, I., and Kunstmann, H.: West African Science Service Centre on Climate Change and Adapted Land Use (WASCAL) High-Resolution Climate
10 Simulation Data. doi: 10.1594/WDCC/WRF60_GFDLESM_HIST, 10.1594/WDCC/WRF60_GFDLESM_RCP45, 10.1594/WDCC/WRF60_HADGEM2_RCP45, 10.1594/WDCC/WRF60_MPIESM_HIST, 10.1594/WDCC/WRF60_MPIESM_RCP45, 10.1594/WDCC/WRF60_ERAINT_CTRL, 10.1594/WDCC/WRF60_HADGEM2_HIST, 10.1594/WDCC/WRF12_ERAINT_CTRL, 10.1594/WDCC/WRF12_MPIESM_RCP45, 10.1594/WDCC/WRF12_GFDLESM_RCP45, 10.1594/WDCC/WRF12_HADGEM2_RCP45, 10.1594/WDCC/WRF12_GFDLESM_HIST, 10.1594/WDCC/WRF12_HADGEM2_HIST, 10.1594/WDCC/WRF12_MPIESM_HIST,
15 https://cera-www.dkrz.de/WDCC/ui/Project.jsp?acronym=WASCAL, 2017a.

Heinzeller, D., Dieng, D., Smiatek, G., Olusegun, C., Klein, C., Hamann, I., and Kunstmann, H.: West African Science Service Centre on Climate Change and Adapted Land Use (WASCAL) high-resolution climate simulation data, links to subset of variables at daily and monthly temporal resolution in NetCDF format, https://doi.org/10.1594/PANGAEA.880512, 2017b.

Jones, C. D., Hughes, J. K., Bellouin, N., Hardiman, S. C., Jones, G. S., Knight, J., Liddicoat, S., O'Connor, F. M., Andres, R. J., Bell, C.,
20 Boo, K. O., Bozzo, A., Butchart, N., Cadule, P., Corbin, K. D., Doutriaux-Boucher, M., Friedlingstein, P., Gornall, J., Gray, L., Halloran, P. R., Hurtt, G., Ingram, W. J., Lamarque, J. F., Law, R. M., Meinshausen, M., Osprey, S., Palin, E. J., Parsons Chini, L., Raddatz, T., Sanderson, M. G., Sellar, A. A., Schurer, A., Valdes, P., Wood, N., Woodward, S., Yoshioka, M., and Zerroukat, M.: The HadGEM2-ES implementation of CMIP5 centennial simulations, Geoscientific Model Development, 4, 543–570, https://doi.org/10.5194/gmd-4-543-2011, 2011.

25 Jung, G. and Kunstmann, H.: High-resolution regional climate modeling for the Volta region of West Africa, Journal of Geophysical Research, 112, 1–17, https://doi.org/10.1029/2006JD007951, 2007.

Kirtman, B., Power, S. B., Adedoyin, J. A., Boer, G. J., Bojariu, R., Camilloni, I., Doblas-Reyes, F. J., Fiore, A. M., Kimoto, M., Meehl, G. A., Prather, M., Sarr, A., Schär, C., Sutton, R., van Oldenborgh, G. J., Vecchi, G., and Wang, H.-J.: Near-term Climate Change: Projections and Predictability, in: Climate Change 2013: The Physical Science Basis. Contribution of Working
30 Group I to the Fifth Assessment Report of the Intergovernmental Panel on Climate Change, edited by Stocker, T., chap. 11, pp. 953–1028, https://doi.org/10.1017/CBO9781107415324.023, https://www.ipcc.ch/pdf/assessment-report/ar5/wg1/WG1AR5_Chapter11_FINAL.pdf, 2013.

Klein, C., Heinzeller, D., Bliefernicht, J., and Kunstmann, H.: Variability of West African monsoon patterns generated by a WRF multi-physics ensemble, Climate Dynamics, https://doi.org/10.1007/s00382-015-2505-5, http://link.springer.com/10.1007/s00382-015-2505-5,
35 2015.

Klein, C., Bliefernicht, J., Heinzeller, D., Gessner, U., Klein, I., and Kunstmann, H.: Feedback of observed interannual vegetation change: a regional climate model analysis for the West African monsoon, Climate Dynamics, 48, 2837–2858, https://doi.org/10.1007/s00382-016-3237-x, 2017.

Laprise, R.: Resolved Scales and Nonlinear Interactions in Limited-Area Models, Journal of the Atmospheric Sciences, 60, 768–779, https://doi.org/10.1175/1520-0469(2003)060<0768:RSANII>2.0.CO;2, http://journals.ametsoc.org/doi/abs/10.1175/1520-0469(2003) 060%3C0768:RSANII%3E2.0.CO%3B2, 2003.

Leduc, M. and Laprise, R.: Regional climate model sensitivity to domain size, Climate Dynamics, 32, 833–854, https://doi.org/10.1007/s00382-008-0400-z, http://link.springer.com/10.1007/s00382-008-0400-z, 2008.

Lee, J. Y. and Wang, B.: Future change of global monsoon in the CMIP5, Climate Dynamics, 42, 101–119, https://doi.org/10.1007/s00382-012-1564-0, 2014.

Lucas-Picher, P., Caya, D., Elía, R., and Laprise, R.: Investigation of regional climate models' internal variability with a ten-member ensemble of 10-year simulations over a large domain, Climate Dynamics, 31, 927–940, https://doi.org/10.1007/s00382-008-0384-8, 2008.

Miguez-Macho, G., Stenchikov, G. L., and Robock, A.: Spectral nudging to eliminate the effects of domain position and geometry in regional climate model simulations, Journal of Geophysical Research D: Atmospheres, 109, https://doi.org/10.1029/2003JD004495, 2004.

Mounkaila, M. S., Abiodun, B. J., and 'Bayo Omotosho, J.: Assessing the capability of CORDEX models in simulating onset of rainfall in West Africa, https://doi.org/10.1007/s00704-014-1104-4, 2014.

Naab, J., Bationo, A., Wafula, B. M., Traore, P. S., Zougmore, R., Ouattara, M., Tabo, R., and Vlek, P. L. G.: African Perspectives on Climate Change and Agriculture: Impacts, Adaptation and Mitigation Potential, pp. 85–106, https://doi.org/10.1142/9781848169845_0006, 2012.

Naabil, E., Lamptey, B. L., Arnault, J., Kunstmann, H., and Olufayo, A.: Water resources management using the WRF-Hydro modelling system: Case-study of the Tono dam in West Africa, Journal of Hydrology: Regional Studies, 12, 196–209, https://doi.org/10.1016/j.ejrh.2017.05.010, 2017.

Neumann, R., Jung, G., Laux, P., and Kunstmann, H.: Climate trends of temperature, precipitation and river discharge in the Volta Basin of West Africa, International Journal of River Basin Management, 5, 17–30, https://doi.org/10.1080/15715124.2007.9635302, 2007.

Niang, I., Ruppel, O., Abdrabo, M., Essel, A., Lennard, C., Padgham, J., and Urquhart, P.: Africa, in: Climate Change 2014: Impacts, Adaptation, and Vulnerability. Part B: Regional Aspects. Contribution of Working Group II to the Fifth Assessment Report of the Intergovernmental Panel on Climate Change, edited by Barros, V., Field, C., Dokken, D., Mastrandrea, M., Mach, K., Bilir, T., Chatterjee, M., Ebi, K., Estrada, Y., Genova, R., Girma, B., Kissel, E., Levy, A., MacCracken, S., Mastrandrea, P., and L.L., W., chap. 22, pp. 1199–1265, Cambridge University Press, https://www.ipcc.ch/pdf/assessment-report/ar5/wg2/WGIIAR5-Chap22_FINAL.pdf, 2014.

Nicholson, S. E.: The West African Sahel: A Review of Recent Studies on the Rainfall Regime and Its Interannual Variability, ISRN Meteorology, 2013, 32, https://doi.org/10.1155/2013/453521, http://www.hindawi.com/isrn/meteorology/2013/453521/abs/, 2013.

Nikulin, G., Jones, C., Giorgi, F., Asrar, G., Büchner, M., Cerezo-Mota, R., Christensen, O. B., Déqué, M., Fernandez, J., Hänsler, A., van Meijgaard, E., Samuelsson, P., Sylla, M. B., and Sushama, L.: Precipitation Climatology in an Ensemble of CORDEX-Africa Regional Climate Simulations, Journal of Climate, 25, 6057–6078, https://doi.org/10.1175/JCLI-D-11-00375.1, http://journals.ametsoc.org/doi/abs/10.1175/JCLI-D-11-00375.1, 2012.

Nikulin, G., Jones, C., Kjellström, E., and Gbobaniyi, E.: The West African Monsoon simulated by global and regional climate models, in: EGU General Assembly 2013, held 7-12 April, 2013 in Vienna, Austria, vol. 15, p. 4581, EGU, http://meetingorganizer.copernicus.org/EGU2013/EGU2013-4581.pdf, 2013.

Noble, E., Druyan, L., and Fulakeza, M.: The sensitivity of WRF daily summertime simulations over West Africa to alternative parameterizations. Part I: african wave circulation., Monthly Weather Review, 142, 1588–1608, https://doi.org/10.1175/MWR-D-13-00194.1, 2014.

Otte, T. L.: The impact of nudging in the meteorological model for retrospective air quality simulations. Part I: Evaluation against national observation networks, Journal of Applied Meteorology and Climatology, 47, 1853–1867, https://doi.org/10.1175/2007JAMC1790.1, 2008.

Otte, T. L., Nolte, C. G., Otte, M. J., and Bowden, J. H.: Does nudging squelch the extremes in regional climate modeling?, Journal of Climate, 25, 7046–7066, https://doi.org/10.1175/JCLI-D-12-00048.1, 2012.

5 Paeth, H., Hall, N. M. J., Gaertner, M. A., Alonso, M. D., Moumouni, S., Polcher, J., Ruti, P. M., Fink, A. H., Gosset, M., Lebel, T., Gaye, A. T., Rowell, D. P., Moufouma-Okia, W., Jacob, D., Rockel, B., Giorgi, F., and Rummukainen, M.: Progress in regional downscaling of west African precipitation, https://doi.org/10.1002/asl.306, 2011.

Park, S.-H., Klemp, J. B., and Skamarock, W. C.: A Comparison of Mesh Refinement in the Global MPAS-A and WRF Models Using an Idealized Normal-Mode Baroclinic Wave Simulation, Monthly Weather Review, 142, 3614–3634, 2014.

10 Rienecker, M. M., Suarez, M. J., Gelaro, R., Todling, R., Bacmeister, J., Liu, E., Bosilovich, M. G., Schubert, S. D., Takacs, L., Kim, G. K., Bloom, S., Chen, J., Collins, D., Conaty, A., Da Silva, A., Gu, W., Joiner, J., Koster, R. D., Lucchesi, R., Molod, A., Owens, T., Pawson, S., Pegion, P., Redder, C. R., Reichle, R., Robertson, F. R., Ruddick, A. G., Sienkiewicz, M., and Woollen, J.: MERRA: NASA's modern-era retrospective analysis for research and applications, Journal of Climate, 24, 3624–3648, https://doi.org/10.1175/JCLI-D-11-00015.1, 2011.

15 Salack, S., Klein, C., Giannini, A., Sarr, B., Worou, O. N., Belko, N., Jan Bliefernicht, and Kunstman, H.: Global warming induced hybrid rainy seasons in the Sahel, Environmental Research Letters, 11, 104 008, https://doi.org/10.1088/1748-9326/11/10/104008, 2016.

Skamarock, W., Klemp, J., Dudhia, J., Gill, D., Barker, D., Duda, M., Huang, X.-Y., Wang, W., and Powers, J.: A Description of the Advanced Research WRF Version 3, Tech. rep., https://doi.org/10.5065/D6DZ069T, 2008.

Skamarock, W. C., Klemp, J. B., Duda, M. G., Fowler, L. D., Park, S.-H., and Ringler, T. D.: A Multiscale Nonhydrostatic Atmospheric
20 Model Using Centroidal Voronoi Tesselations and C-Grid Staggering, https://doi.org/10.1175/MWR-D-11-00215.1, 2012.

Stevens, B., Giorgetta, M., Esch, M., Mauritsen, T., Crueger, T., Rast, S., Salzmann, M., Schmidt, H., Bader, J., Block, K., Brokopf, R., Fast, I., Kinne, S., Kornblueh, L., Lohmann, U., Pincus, R., Reichler, T., and Roeckner, E.: Atmospheric component of the MPI-M earth system model: ECHAM6, Journal of Advances in Modeling Earth Systems, 5, 146–172, https://doi.org/10.1002/jame.20015, 2013.

Strandberg, G., Bärring, L., Hansson, U., Jansson, C., Jones, C., Kjellström, E., Kolax, M., Kupiainen, M., Nikulin, G., Samuelsson, P.,
25 Ullerstig, A., and Wang, S.: SMHI Report Meteorology and Climatology No. 116, Tech. rep., 2014.

Sylla, M. B., Giorgi, F., Coppola, E., and Mariotti, L.: Uncertainties in daily rainfall over Africa: Assessment of gridded observation products and evaluation of a regional climate model simulation, International Journal of Climatology, 33, 1805–1817, https://doi.org/10.1002/joc.3551, 2013.

Sylla, M. B., Giorgi, F., Pal, J. S., Gibba, P., Kebe, I., and Nikiema, M.: Projected changes in the annual cycle of high-intensity precipitation
30 events over West Africa for the late twenty-first century, Journal of Climate, 28, 6475–6488, https://doi.org/10.1175/JCLI-D-14-00854.1, 2015.

Sylla, M. B., Elguindi, N., Giorgi, F., and Wisser, D.: Projected robust shift of climate zones over West Africa in response to anthropogenic climate change for the late 21st century, Climatic Change, 134, 241–253, https://doi.org/10.1007/s10584-015-1522-z, 2016.

Taylor, K. E., Stouffer, R. J., and Meehl, G. A.: An overview of CMIP5 and the experiment design, https://doi.org/10.1175/BAMS-D-11-
35 00094.1, 2012.

van Vuuren, D. P., Edmonds, J., Kainuma, M., Riahi, K., Thomson, A., Hibbard, K., Hurtt, G. C., Kram, T., Krey, V., Lamarque, J. F., Masui, T., Meinshausen, M., Nakicenovic, N., Smith, S. J., and Rose, S. K.: The representative concentration pathways: An overview, Climatic Change, 109, 5–31, https://doi.org/10.1007/s10584-011-0148-z, 2011.

von Storch, H., Langenberg, H., and Feser, F.: A Spectral Nudging Technique for Dynamical Downscaling Purposes, https://doi.org/10.1175/1520-0493(2000)128<3664:ASNTFD>2.0.CO;2, 2000.

Warner, T. T., Peterson, R. A., and Treadon, R. E.: A Tutorial on Lateral Boundary Conditions as a Basic and Potentially Serious Limitation to Regional Numerical Weather Prediction, Bulletin of the American Meteorological Society, 78, 2599–2617, https://doi.org/10.1175/1520-0477(1997)078<2599:ATOLBC>2.0.CO;2, 1997.

Willmott, C. J. and Matsuura, K.: Terrestrial Air Temperature and Precipitation: Monthly and Annual Time Series (1900 - 2010), http://climate.geog.udel.edu/~climate/html_pages/README.ghcn_ts2.html, 2012.

World Meteorological Organization: Guide to Climatological Practices, 3rd edition edn., http://www.wmo.int/pages/prog/wcp/ccl/documents/WMO_100_en.pdf, 2011.

5

Table 7. Re-analyses and global circulation models (earth system models) used as forcing data for the long-term regional climate simulations, and regional climate model used to conduct the ensemble experiment. The characteristics of the forcing models for Africa and their climate change signal (CCS) are taken from Elguindi et al. (2014); OBS denotes observations, MMM the CMIP5 multi-model ensemble mean.

GCM/ESM	Characteristics for West Africa	CCS	Reference
ERA-Interim	re-analysis, "perfect atmosphere"	—	Dee et al. (2011)
MPI-ESM MR	temp. close to OBS/MMM	medium	Stevens et al. (2013)
HadGEM2-ES	precip. close to OBS/MMM	large	Jones et al. (2011)
GFDL-ESM2M	both differ from OBS/MMM	small	Anon (2012)
RCM	**Model configuration for West Africa**		**Reference**
WRFV3.5.1	see Table 9		Skamarock et al. (2008)

Table 8. Computational resources used for the WASCAL high-resolution regional climate ensemble experiment. Control runs are conducted for the period 1979–2014, historical runs for the period 1979–2010 (for details, see text), and RCP4.5 projection runs for the periods 2019–2050 and 2069–2100.

GCM/ESM	RCM	Experiment	HPC
ERA-Interim	WRFV3.5.1	control	DKRZ Blizzard
MPI-ESM MR	WRFV3.5.1	hist./proj.	JSC Juropa
GFDL-ESM2M	WRFV3.5.1	hist./proj.	JSC Juropa
HadGEM2-ES	WRFV3.5.1	hist./proj.	JSC Jureca
Preprocessing			KIT/IMK-IFU Kea
Postprocessing			DKRZ Mistral

DKRZ: German Climate Computing Centre, http://www.dkrz.de; JSC: Jülich Supercomputing Centre of the Research Centre Jülich, http://www.fz-juelich.de/ias/jsc; SCC: Steinbruch Centre for Computing of the Karlsruhe Institute of Technology, http://scc.kit.edu.

**Table 9.** WRF model configuration for the two domains at 60 km and 12 km resolution.

Run	wrf-60km	wrf-12km
Microphysics	WSM5	WSM5
Radiation	RRTMG LW/SW	RRTMG LW/SW
Cumulus	Grell-Devenyi	Grell-Devenyi
PBL	ACM2 (Pleim)	ACM2 (Pleim)
Surface layer	Janjic Eta	Janjic Eta
Land-surface	Noah LSM	Noah LSM
Grid FDDA	UV/T/PH above PBL	off
o3input	2	2
aer_opt	1	1
Domain size	$157 \times 106 \times 40$	$496 \times 331 \times 40$
Time step	360 s	72 s
Rad. time step	24 m	24 m
LBC[*] interval	6 h	3 h

[*]Lateral Boundary Conditions

**Table 10.** Available data at CERA (https://cera-www.dkrz.de/WDCC/ui/Project.jsp?acronym=WASCAL) and PANGAEA. Note that the former URL opens a search mask on the CERA database for all available data sets (ensemble members), while the links behind the individual DOIs pre-select the corresponding ensemble member. On PANGAEA, a single DOI is assigned to the data from all ensemble members.

DOI	Description
Data available at CERA	
10.1594/WDCC/WRF12_ERAINT_CTRL	12 km resolution, forcing ERA-Interim, control run 1979–2014
10.1594/WDCC/WRF12_GFDLESM_HIST	12 km resolution, forcing GFDL-ESM2M, historical run 1979–2005
10.1594/WDCC/WRF12_GFDLESM_RCP45	12 km resolution, forcing GFDL-ESM2M, RCP4.5 run 2006–2100
10.1594/WDCC/WRF12_HADGEM2_HIST	12 km resolution, forcing HadGEM2-ES, historical run 1979–2005
10.1594/WDCC/WRF12_HADGEM2_RCP45	12 km resolution, forcing HadGEM2-ES, RCP4.5 run 2006–2100
10.1594/WDCC/WRF12_MPIESM_HIST	12 km resolution, forcing MPI-ESM MR, historical run 1979–2005
10.1594/WDCC/WRF12_MPIESM_RCP45	12 km resolution, forcing MPI-ESM MR, RCP4.5 run 2006–2100
10.1594/WDCC/WRF60_ERAINT_CTRL	60 km resolution, forcing ERA-Interim, control run 1979–2014
10.1594/WDCC/WRF60_GFDLESM_HIST	60 km resolution, forcing GFDL-ESM2M, historical run 1979–2005
10.1594/WDCC/WRF60_GFDLESM_RCP45	60 km resolution, forcing GFDL-ESM2M, RCP4.5 run 2006–2100
10.1594/WDCC/WRF60_HADGEM2_HIST	60 km resolution, forcing HadGEM2-ES, historical run 1979–2005
10.1594/WDCC/WRF60_HADGEM2_RCP45	60 km resolution, forcing HadGEM2-ES, RCP4.5 run 2006–2100
10.1594/WDCC/WRF60_MPIESM_HIST	60 km resolution, forcing MPI-ESM MR, historical run 1979–2005
10.1594/WDCC/WRF60_MPIESM_RCP45	60 km resolution, forcing MPI-ESM MR, RCP4.5 run 2006–2100
Data available at PANGAEA	
10.1594/PANGAEA.880512	subset of all 12 km data for selected variables at daily or monthly temporal resolution
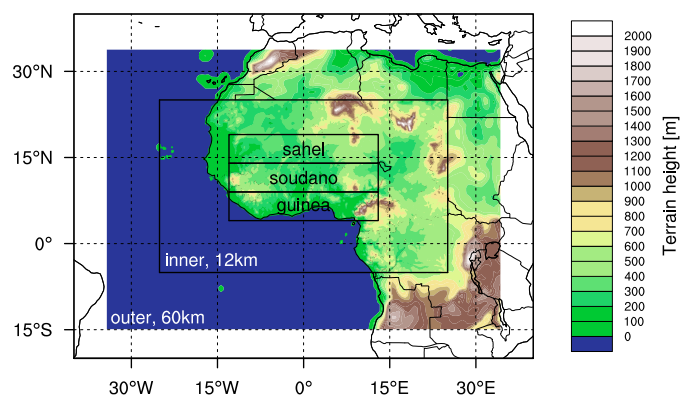
Figure 1. Nested domain configuration with 60 km and, 12 km. Also shown are three distinct agro-climatical regions used in the analysis.

Open Access

Earth System
Science
Data

Discussions
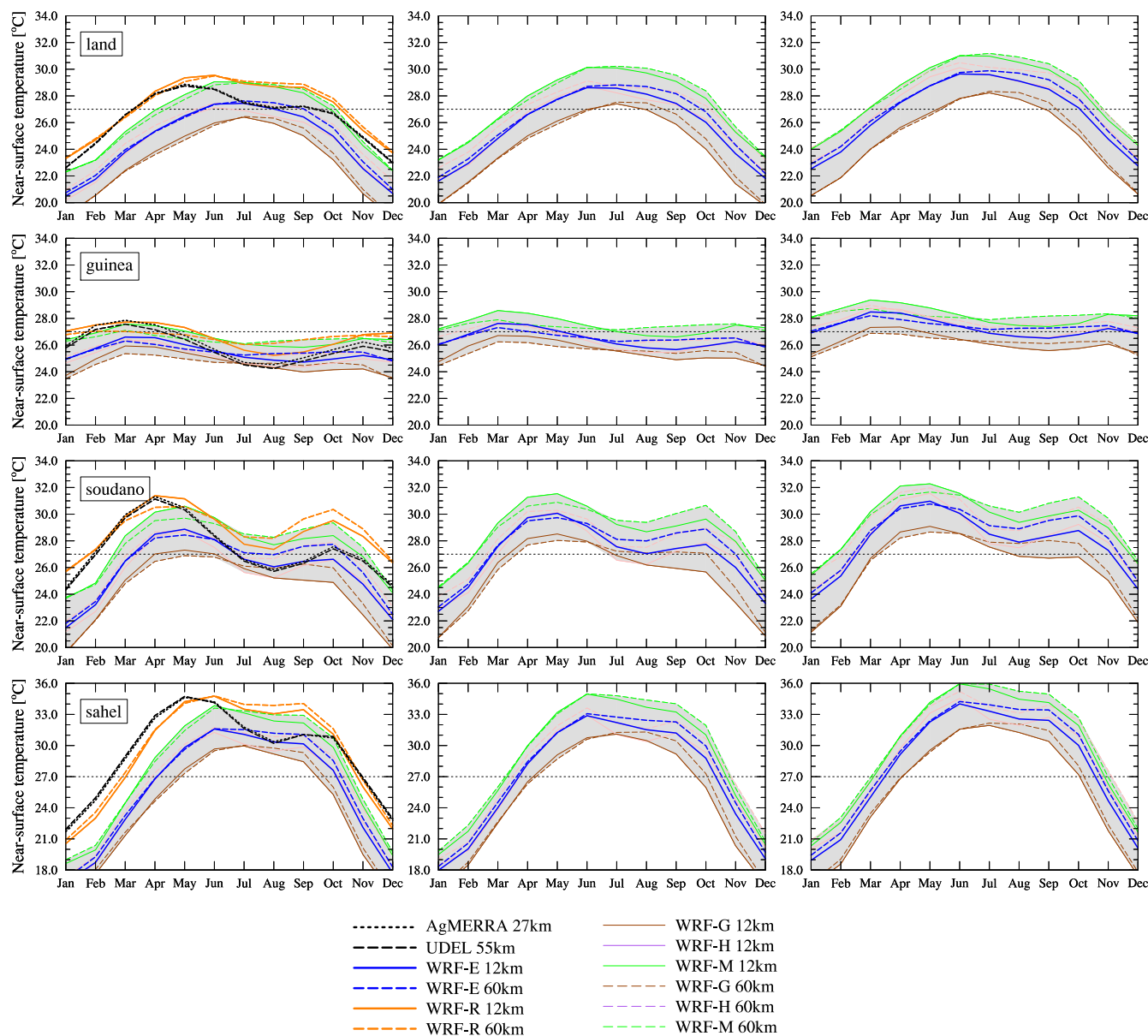
Figure 2. Annual cycle of near-surface temperature for the historical period 1980–2010 (left), the near future 2020–2050 (middle) and the end of the 21st century 2070–2100 (right), averaged over all land area and for the different regions displayed in Fig. 1. WRF-R: ERA-Interim control run; WRF-M: MPI-ESM MR historical run; WRF-H: HadGEM2-ES historical run; WRF-G: GFDL-ESM2M historical run; WRF-E: multi-model ensemble of WRF-M, WRF-H and WRF-E. The shaded areas encompass the entire spread of the 12 km and 60 km members of the multi-model ensembles.
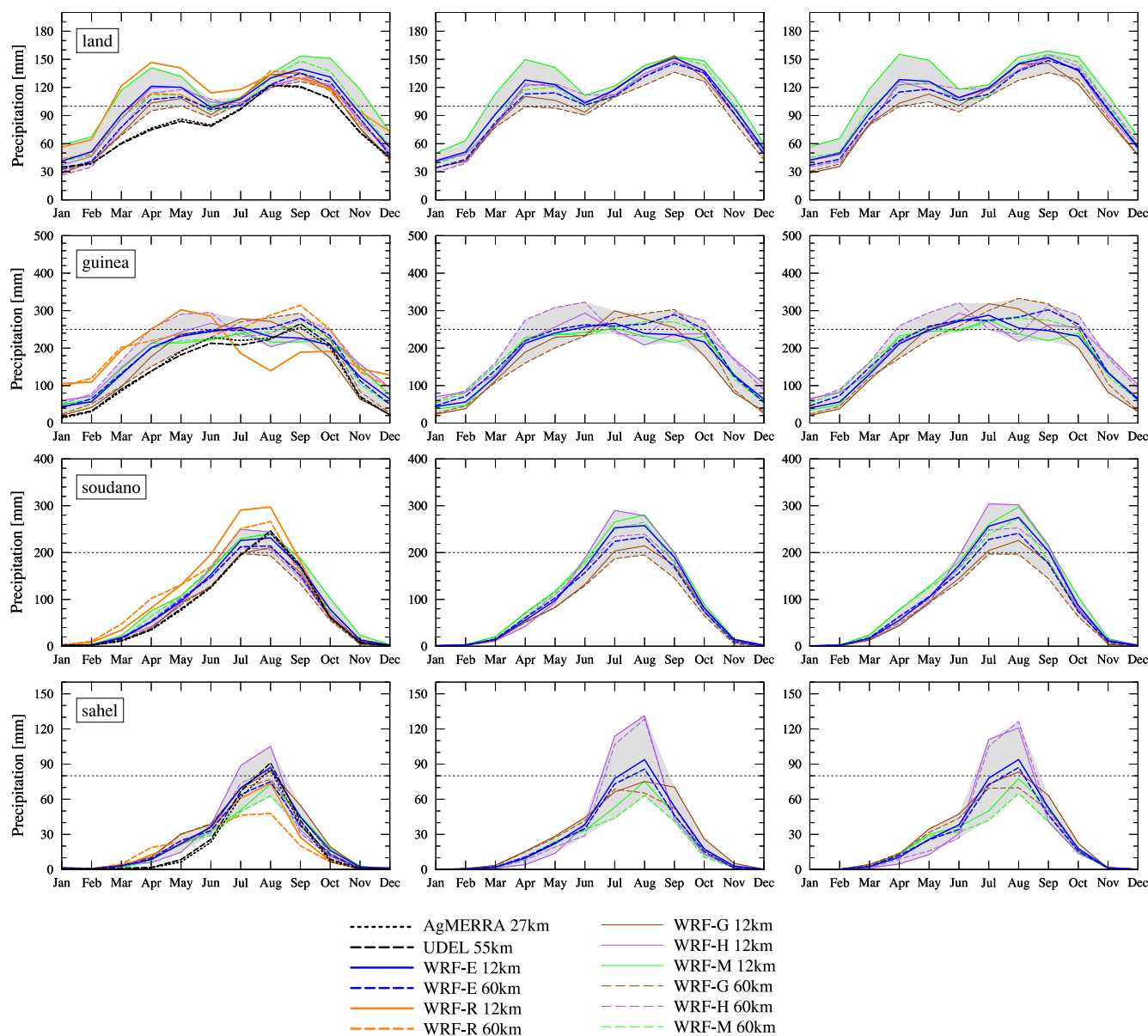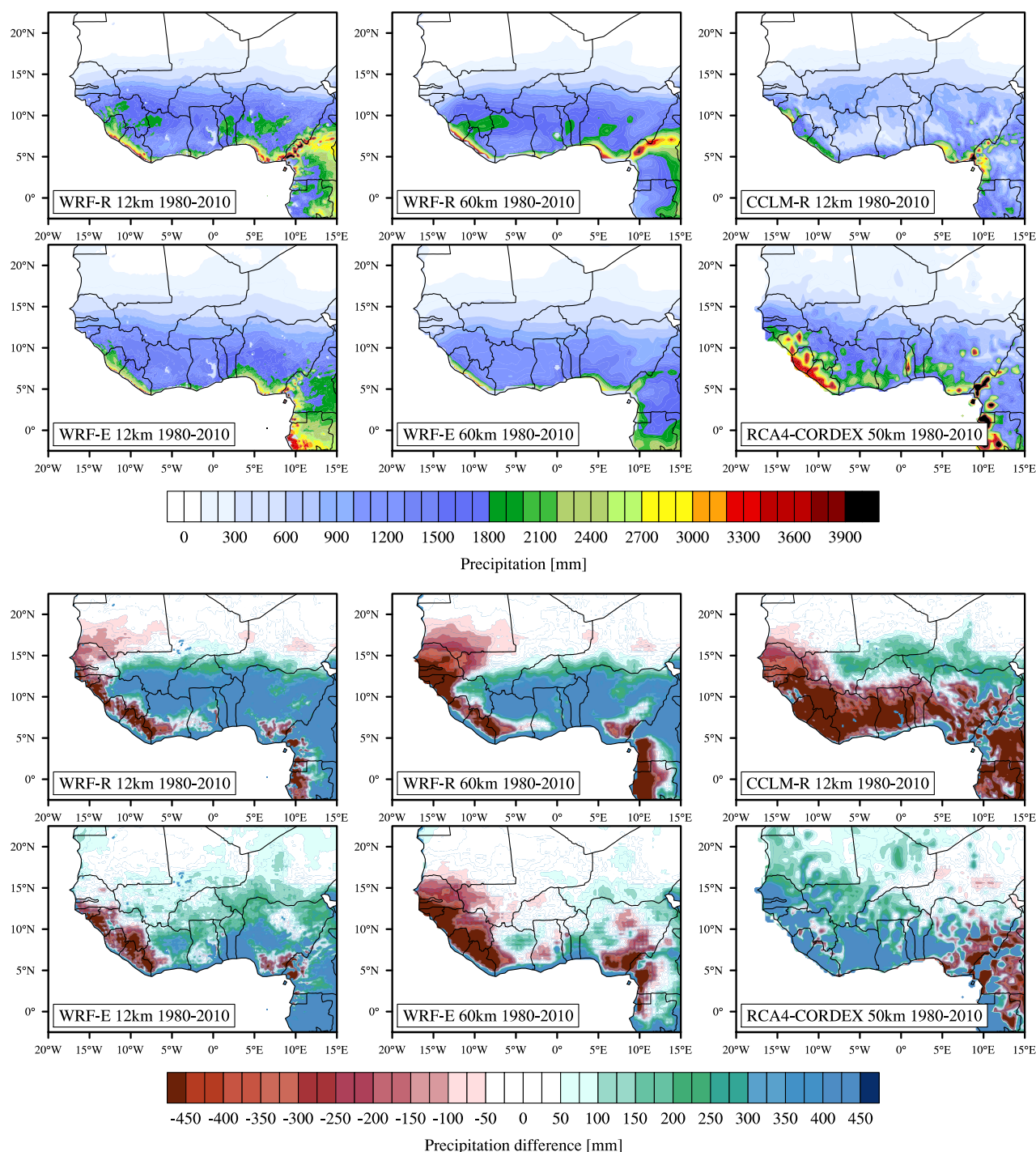
Figure 3. Annual cycle of precipitation for the historical period 1980–2010 (left), the near future 2020–2050 (middle) and the end of the 21st century 2070–2100 (right), averaged over all land area and for the different regions displayed in Fig. 1. WRF-R: ERA-Interim control run; WRF-M: MPI-ESM MR historical run; WRF-H: HadGEM2-ES historical run; WRF-G: GFDL-ESM2M historical run; WRF-E: multi-model ensemble of WRF-M, WRF-H and WRF-E. The shaded areas encompass the entire spread of the 12 km and 60 km members of the multi-model ensembles.
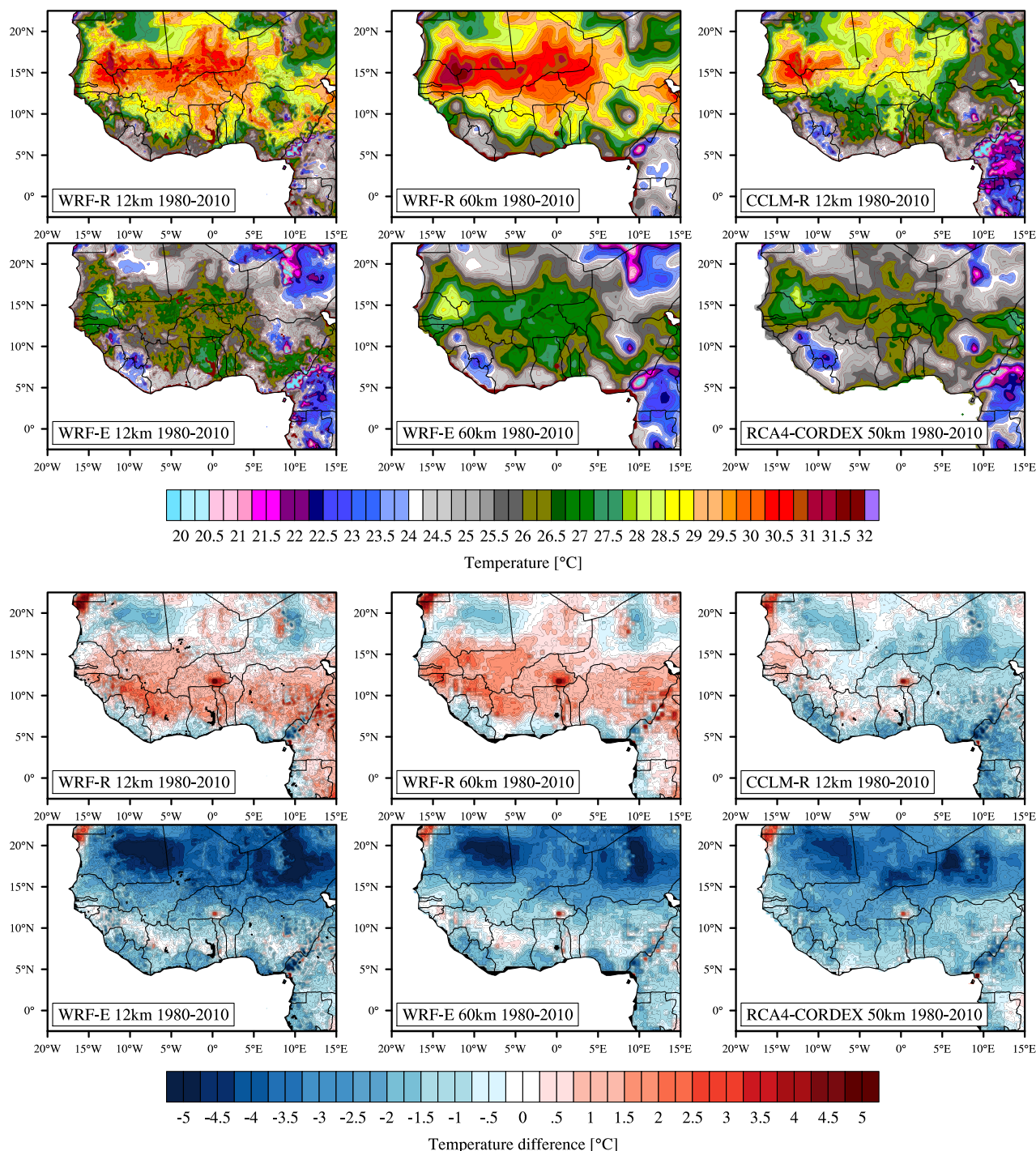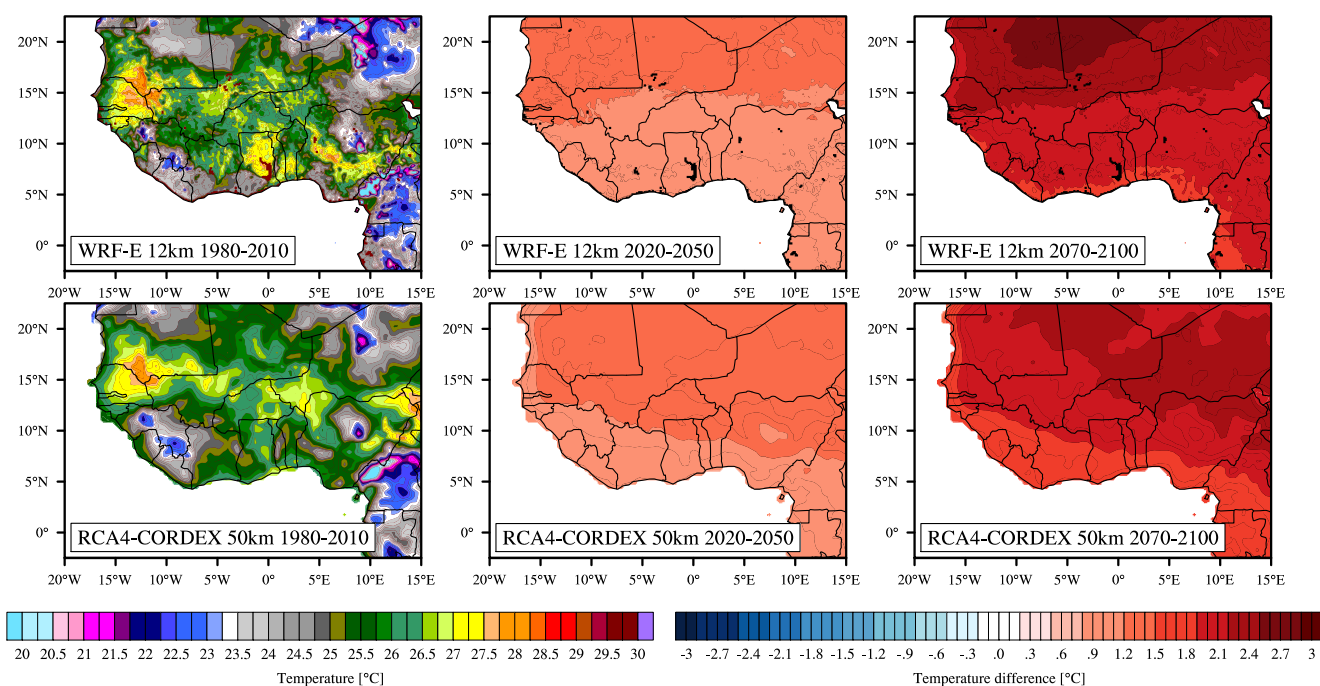
Figure 4. Near-surface temperature averaged over the historical reference period 1980–2010 (top panels) and differences to AgMERRA re-analysis data (lower panels) for the WRF control runs WRF-R, the WRF multi-model ensemble WRF-E, a CCLM control run CCLM-R and a two-member ensemble RCA4-CORDEX.
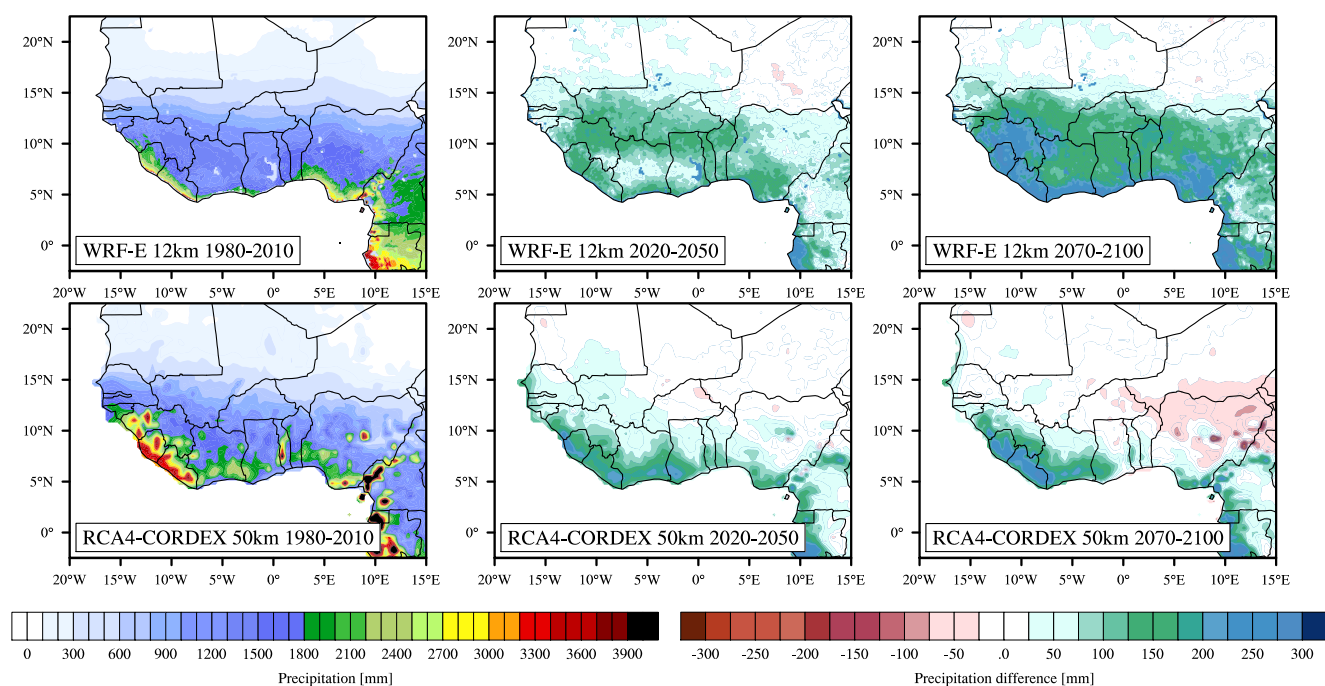
Figure 5. Annual precipitation averaged over the historical reference period 1980–2010 (top panels) and differences to AgMERRA reanalysis data (lower panels) for the WRF control runs WRF-R, the WRF multi-model ensemble WRF-E, a CCLM control run CCLM-R and a two-member ensemble RCA4-CORDEX.

Figure 6. Near-surface temperature averaged over the historical reference period 1980–2010 (left) and climate change signal for the near future 2020–2050 (middle) and the end of the 21st century 2070–2100 (right) for the WRF multi-model ensemble WRF-E and a two-member ensemble RCA4-CORDEX.

Figure 7. Annual precipitation averaged over the historical reference period 1980–2010 (left) and climate change signal for the near future 2020–2050 (middle) and the end of the 21st century 2070–2100 (right) for the WRF multi-model ensemble WRF-E and a two-member ensemble RCA4-CORDEX.